Aerosol transport pathways and source attribution in China during the COVID-19 outbreak

Lili Ren[1], Yang Yang[1*], Hailong Wang[2], Pinya Wang[1], Lei Chen[1], Jia Zhu[1], Hong Liao[1]

[1]Jiangsu Key Laboratory of Atmospheric Environment Monitoring and Pollution Control, Jiangsu Collaborative Innovation Center of Atmospheric Environment and Equipment Technology, School of Environmental Science and Engineering, Nanjing University of Information Science and Technology, Nanjing, Jiangsu, China

[2]Atmospheric Sciences and Global Change Division, Pacific Northwest National Laboratory, Richland, Washington, USA

*Correspondence to yang.yang@nuist.edu.cn

Abstract

Due to the coronavirus disease 2019 (COVID-19) pandemic, human activities and industrial productions were strictly restricted during January-March 2020 in China. Despite the fact that anthropogenic aerosol emissions largely decreased, haze events still occurred. Characterization of aerosol transport pathways and attribution of aerosol sources from specific regions are beneficial to the air quality and pandemic control strategies. This study establishes source-receptor relationships in various regions covering the whole China during the COVID-19 outbreak based on the Community Atmosphere Model version 5 with Explicit Aerosol Source Tagging (CAM5-EAST). Our analysis shows that $PM_{2.5}$ burden over the North China Plain between January 30 and February 19 is mostly contributed by local emissions (40–66%). For other regions in China, $PM_{2.5}$ burden is largely contributed from non-local sources. During the most polluted days of COVID-19 outbreak, local emissions within North China Plain and Eastern China, respectively, contribute 66% and 87% to the increase in surface $PM_{2.5}$ concentrations. This is associated with the anomalous mid-tropospheric high pressure at the location of climatological East Asia trough and the consequently weakened winds in the lower troposphere, leading to the local aerosol accumulation. The emissions outside China, especially those from South and Southeast Asia, contribute over 50% to the increase in $PM_{2.5}$ concentration in Southwestern China

through transboundary transport during the most polluted day. As the reduction in emissions in the near future, aerosols from long-range transport together with unfavorable meteorological conditions are increasingly important to regional air quality and need to be taken into account in clean air plans.

1. Introduction

The coronavirus disease 2019 (COVID-19) has spread worldwide since December 2019 and resulted in more than one million cases within the first four months (Sharma et al., 2020; Dong et al., 2020). In order to curb the virus spread among humans, measures were taken by the Chinese government on January 23, 2020 to minimize the interaction among people, including strict isolation, prohibition of large-scale private and public gatherings, restriction of private and public transportation and even lockdown of cities (Tian et al., 2020; Wang et al., 2020).The estimated NOx emission in eastern China was reduced by 60-70%, of which 70-80% was related to the reduced road traffic and 20-25% was from industrial enterprises shutdown during the COVID-19 lockdown period. However, severe air pollution events still occurred in East China during the COVID-19 lockdown, even though the anthropogenic emissions were greatly reduced (Huang et al., 2020). The unprecedented large-scale restrictions resulting from the COVID-19 epidemic provide an opportunity to research the relationship between dramatic anthropogenic emission reductions and air quality changes (e.g., Bao et al., 2020; Li et al., 2020; Wang et al., 2020). Bao et al. (2020) reported that, during the COVID-19 lockdown period, the air quality index and the $PM_{2.5}$ (particulate matter less than 2.5 μm in diameter) concentration were decreased by 7.8% and 5.9 %, respectively, on average in 44 cities in northern China, mainly due to travel restrictions.

By applying the WRF-CAMx model together with air quality monitoring data, Li et al. (2020) revealed that although primary particle emissions were reduced by 15%–61% during the COVID-19 lockdown over the Yangtze River Delta Region, the daily mean concentration of $PM_{2.5}$ was still relatively high, reaching up to 79 μg m^{-3}. Wang et al. (2020) found that the relative reduction in $PM_{2.5}$ precursors was twice as much as the reduction in $PM_{2.5}$ concentration, in part due to the unfavorable meteorological conditions during the COVID-19 outbreak in China that led to the formation of the heavy haze. Huang et al. (2020) and Le et al. (2020) reported that stagnant air conditions, high atmospheric humidity, and enhanced atmospheric oxidizing capacity led to a severe haze event in northern China during the COVID-19 pandemic.

Aerosols are main air pollutants that play important roles in the atmosphere due to their adverse effects on air quality, visibility (Vautard et al., 2009; Watson, 2002), human health (Lelieveld et al., 2019; Heft-Neal et al., 2018), the Earth's energy balance, and regional and global climate (Ramanathan et al., 2001; Anderson et al., 2003; Wang et al., 2020; Smith et al., 2020). With the rapid development in recent decades, China has experienced severe air pollutions that damage human health and cause regional climate change (Chai et al., 2014; Liao et al., 2015; Fan et al., 2020). In order to control air pollution, the Chinese government issued and implemented the Air Pollution Prevention and Control Action Plan in 2013

(China State Council, 2013). Although emissions in China have decreased significantly in recent years (Zheng et al., 2018), aerosols transported from other source regions could add on top of local emissions (Yang et al., 2017a, 2018a; Ren et al., 2020). Therefore, it is important to understand the relative effects of local emissions and regional transport on aerosols in China.

Source tagging and apportionment is an effective way to establish aerosol source-receptor relationships, which is conducive to both scientific research and emission control strategies (Yu et al., 2012). By applying the Particulate Source Apportionment Technology in CAMx model, Xue et al. (2014) found that the contributions of regional transport to annual average $PM_{2.5}$ concentrations in Hainan, Shanghai, Jiangsu, Zhejiang, Jilin and Jiangxi provinces of China are more than 45%. By adding a chemical tracer into the WRF model, Wang et al. (2016) studied the sources of black carbon (BC) aerosol in Beijing and reported that about half of BC in Beijing came from the central North China Plain. Liu et al. (2017) applied WRF-Chem model and showed that Foshan, Guangzhou and Dongguan, respectively, with relatively high emissions contributed 14%, 13% and 10% to the regional mean $PM_{2.5}$ concentration in the Pearl River Delta.

Currently, previous studies only focused on regional transport of aerosols, very few studies have explored the aerosol transport pathways and source attribution covering the whole China during the COVID-19 pandemic. In this study, the global aerosol-climate model CAM5 (Community Atmosphere Model, version 5) equipped with an Explicit Aerosol Source Tagging (CAM5-EAST) is employed to quantify source-receptor relationships and transport pathways of aerosols during the COVID-19 outbreak in China. We also provide model evaluations of $PM_{2.5}$ concentrations against observations made during the COVID-19 outbreak. With the aerosol source tagging technique, source region contributions to $PM_{2.5}$ column burden over various receptor regions and transport pathways in China are analyzed. The source contributions to the changes in near-surface $PM_{2.5}$ in the most polluted days compared to the monthly means during February 2020 are also quantified. Our study provides source apportionment of aerosols covering the whole China and quantifies the contribution from foreign transport for the first time in the case of COVID-19 emission reductions, which is beneficial to the investigation of policy implications for future air pollution control.

2. Methods

2.1 Model description and experimental setup

The CAM5 model is applied to estimate the $PM_{2.5}$ changes during the COVID-19 period, which is the atmospheric component of the earth system model CESM (Community Earth System Model, Hurrell et al., 2013). In this study, major aerosol species including sulfate, BC, primary organic matter (POM), secondary organic aerosol (SOA), sea salt, and mineral dust, are represented by three lognormal size modes (i.e., Aitken, accumulation, and coarse modes) of the modal aerosol module (MAM3) (Liu et al., 2012). The detailed aerosol representation in CAM5 was provided in Liu et al. (2012) and Wang et al. (2013). The aerosol mixing states consider both internal mixed (within a same mode) and external mixed (between modes). On top of the default CAM5, additional modifications that improve the representation of aerosol wet scavenging and convective transport (Wang et al., 2013) are also included in the model version used for this study.

In this study, simulations were conducted with a horizontal resolution of 1.9° × 2.5° and 30 vertical layers up to 3.6 hPa in year 2020. The anthropogenic emissions used in the baseline simulation are derived from the MEIC (Multi-resolution Emission Inventory of China) inventory (Zheng et al., 2018), referred to here as the Baseline experiment. While emissions for the other countries use the SSP (Shared Socioeconomic Pathways) 2–4.5 scenario data set under CMIP6 (the Coupled Model Intercomparison Project Phase 6). Emissions in year 2017 are used as the baseline during the simulation period considering the time limit of MEIC inventory. To better estimate the impact of restricted human activities on emission reductions owing to COVID-19 lockdown (referred to as Covid experiment), we updated China’s emission inventory from January to March 2020 based on the provincial total emission reduction ratio in Huang et al. (2020). Emissions from the transportation sector are decreased by 70%. The remaining emission reduction, by excluding transport reduction from the total emission reduction, are evenly distributed to other sectors, including industry, power plant, residential, international shipping and waste treatment from January to March 2020 compared to the baseline emission in 2017. Unless otherwise specified， all the results in this study are derived from the Covid experiment.

The sea surface temperature, sea ice concentrations, solar radiation and greenhouse gas concentrations are fixed at present-day climatological levels. To capture the large-scale atmospheric circulations during the COVID-19, we nudge the model wind fields toward the MERRA-2 (Modern-Era Retrospective Analysis for Research and Applications, version 2) reanalysis (Gelaro et al., 2017) from April 2019 to March 2020 repeatedly for six years. Only model results from the last year are used to represent year 2020 with the first five years as model spin-up. In this study, we analyze the transport pathways and source attribution of aerosols during the three weeks that had the largest number of newly-diagnosed COVID-19 cases (Fig. S1, hereafter referred to as the 'Week 1': January 30–February 5, 'Week 2': February 6–February 12 and 'Week 3': February 13–February 19), when unexpected hazardous air pollution events also occurred during this time period (Huang et al., 2020; Le et al., 2020).

2.2 Explicit aerosol source tagging and source regions

To examine the source apportionment of aerosols in China, the Explicit Aerosol Source Tagging (EAST) technique was implemented in CAM5, which has been utilized in many aerosol source attribution studies (e.g., Wang et al., 2014; Yang et al., 2017a, b, 2018a, b, c, 2020; Ren et al., 2020). Different from the emission sensitivity method that assumes a linear response to emission perturbation and the traditional backward trajectory method, aerosols from each tagged region or sector are calculated independently in EAST within one single simulation. Without relying on a set of model simulations with emission perturbations or assuming constant decaying rate, EAST is more accurate and time-saving than the source apportionment method mentioned above. In addition to the sulfate, BC and POM species that were tagged in previous studies (e.g., Yang et al., 2020), SOA and precursor gas are now also tagged in the EAST. These types of aerosols from independent source regions and sectors can be explicitly tagged and tracked simultaneously. In this study, focusing on the aerosols in China during the COVID-19 outbreak period, the domestic aerosol and precursor emissions from eight geographical source regions (Fig. 1), including Northeastern China (NEC), North China Plain (NCP), Eastern China (ESC), Southern China (STC), Central-West China (CWC), Southwestern China (SWC), Northwestern China (NWC) and the Himalayas and Tibetan Plateau (HTP), and the rest of the world (ROW), are tagged separately.

3. Model evaluation

Many previous studies have assessed the spatial distribution and seasonal to decadal variations in aerosol concentrations in China and worldwide simulated by CAM5 with the observations (e.g., Wang et al., 2013; Yang et al., 2017a,b, 2018b,c, 2020). In order to evaluate the model's performance in simulating aerosols during the COVID-19 outbreak period in China, the surface concentrations of $PM_{2.5}$, estimated as the sum of sulfate, BC, POM and SOA for model results, during the analyzed time periods are compared with measurements from the China National Environmental Monitoring Center (CNEMC), as shown in Fig. 2a. The model reasonably reproduces the overall spatial distribution of near-surface $PM_{2.5}$ concentrations during the three time periods, with high values in the North China Plain and low values in western China. However, as reported in many CAM5 model studies (e.g., Yang et al., 2017a,b), the model underestimates the $PM_{2.5}$ concentrations with normalized mean biases (NMB) of -55%~-49%, compared to the available site observations (Fig. S2). The discrepancies are related to coarse-resolution model sampling bias relative to the observational sites, uncertainties in aerosol emissions, wet removal, and gas-particle exchange. In addition, the model version used in this study is not able to simulate nitrate and ammonium aerosols, which are also the main components of $PM_{2.5}$ (Kong et al., 2020; Xu et al., 2019).

The long-distance transport of aerosols mainly occurs in the upper troposphere rather than near the surface (Hadley et al., 2007; Zhang et al., 2015). Aerosols are lifted from the atmospheric boundary layer of the emission source regions to the free troposphere and then undergo the transboundary and intercontinental transport effectively driven by the upper tropospheric circulations. Therefore, it is helpful to analyze the relative contributions of local and non-local sources by focusing on the column burden of aerosols. Figure 2b presents spatial distributions of simulated mean column burden of $PM_{2.5}$ during the three time periods ('Week 1': January 30–February 5, 'Week 2': February 6–February 12 and 'Week 3': February 13–February 19), which had the largest number of newly-diagnosed COVID-19 cases. The contrast in column burden does not differ significantly from that of near-surface concentrations. Comparing to Week 3, Week 1 and Week 2 have higher $PM_{2.5}$ loading, with values in the range of 20–40 and 20–30 mg m^{-2} in the North China Plain, Eastern China, and Southern China, while the $PM_{2.5}$ loading in Week 3 is relative lower with than Week 1 and Week 2 with values ranging mostly from 10 to 20 mg m^{-2}. Note that the column burden of $PM_{2.5}$ in South and Southeast Asia is higher than 20 mg m^{-2} in three time periods and reaches up to 50 mg m^{-2} in Week 2, which potentially influences aerosol concentrations in China through transboundary transport.

4. Transport Pathways

The explicit aerosol tagging technique can clearly identify the transport pathways of aerosols moving from their source regions to their destination. Figure 3 shows the spatial distribution of mean column burden of simulated $PM_{2.5}$ originating from the six tagged source regions in central and eastern China and outside of China during the three time periods. Aerosols and/or precursor gases emitted from the various regions follow quite different transport pathways determined by their source locations, meteorological conditions, emission injection height, and physical and chemical characteristics of aerosol species. Aerosols from Northeastern China are transported southeastward by the northwesterly winds (Fig. 1b). From the North China Plain, aerosols can be transported either southward reaching Eastern, Southern and Southwestern China during Week 1 or across east coast of China to the oceanic region during Week 2-3. Aerosols originating from Eastern China move straight to Southwestern and Southern China during Week 1-2, while they also entered the North China Plain during Week 2-3. Aerosols emitted from Southern China and Central-West China have no obvious transport due to their relatively weak emissions. In additional to the local impact, emissions from Southwestern China affect mostly the Southern China and Eastern China. Air parcels with high levels of $PM_{2.5}$ from South and Southeast Asia moved into Southwestern, Southern and Eastern China and even the North China Plain during the three time periods.

The vertical distributions of $PM_{2.5}$ emitted from six major tagged source regions are shown in Figs. S3 and S4. The $PM_{2.5}$ has much higher concentrations in the lower troposphere and decreases with increasing height. During Week 1-2, owing to the presence of high $PM_{2.5}$ loadings, a stronger vertical mixing and transport brought more $PM_{2.5}$ to the upper troposphere compared to that during Week 3. High concentrations of $PM_{2.5}$ originating from the North China Plain extended southeastward by strong northwesterly winds. Weak winds over Eastern China led to accumulations of $PM_{2.5}$ within this region, which is consistent with the findings in Yang et al. (2017a). Strong southwesterly winds in the south of Southwestern China and weak winds in the north of this region produced convergences and updrafts that lift aerosols up to 700 hPa.

Considering that the emissions outside China contribute greatly to $PM_{2.5}$ concentrations in Southwestern China through transboundary transport (Yang et al., 2017a) and aerosols from East Asia can be transported to the North Pacific and even North America (Yu et al., 2008; Yang et al., 2018c), it is of great importance to study the inflow and outflow of $PM_{2.5}$ across the boundaries of China. Figures 4 and 5 show the vertical distribution of $PM_{2.5}$ concentrations resulting from emissions within and outside China over 29°N，88°E and 21°N around the south boundaries (cross-sections (CS) 1-3 in Fig. 1a) and 123° E around the east boundary (CS 4 in Fig. 1a) of the mainland of China. Over the southern border, $PM_{2.5}$

concentrations are more influenced by transboundary transport of aerosols from ROW than those originating from domestic emissions. The high concentrations of $PM_{2.5}$ from South and Southeast Asia are lifted into the free atmosphere of the Tibetan Plateau and Yun-Gui Plateau, and then transported to Southern and Southwestern China by southwesterly winds. Over the North China Plain and Eastern China, northwesterly winds at 35-45° N and southwesterly winds at 25-35° N cause aerosols to accumulate in the lower atmosphere and then export across east border of China below 700 hPa.

5. Source apportionment of $PM_{2.5}$ in China during the COVID-19

5.1 Source contributions to $PM_{2.5}$ burden

Figure 6 shows the simulated relative contributions in percentage to $PM_{2.5}$ column burden from local source emissions, regional transport from the untagged regions of China (rest of China, RCN) and rest of the world (ROW). Over the North China Plain, where emissions are relatively high, $PM_{2.5}$ column burden is dominated by local emissions during the three time periods. In contrast, regions with relative low emissions are mainly affected by nonlocal sources, especially by foreign contributions. Emissions from the ROW contribute a large amount to $PM_{2.5}$ burden over Northeastern, Southern, Central-West, Southwestern, Northwestern China and the Tibetan Plateau. $PM_{2.5}$ burden in Eastern China is greatly contributed by the sources from RCN, especially in Week 1 when regional transport of $PM_{2.5}$ from the North China Plain is relatively strong (Fig. S4).

Table 1 summarizes the contributions of tagged source regions to the $PM_{2.5}$ burden over different receptor regions in China. In Northeastern China, 36%-43% of the $PM_{2.5}$ column burden comes from local emissions, while a larger portion (39%-54%) is contributed by emissions from ROW during the three time periods. The impacts of nonlocal sources within China on $PM_{2.5}$ burden are relatively low in Northeastern China during Week 1 with the contribution of less than 5%, while RCN is responsible for 23% and 25% during Week 2 and Week 3, respectively.

In the North China Plain, the majority of the $PM_{2.5}$ burden is attributed to local emissions in all cases, with local contributions in a range of 40–66%. Emissions from the North China Plain also produce a widespread impact on $PM_{2.5}$ over its neighboring regions. The sources from North China Plain account for 14–33% of the $PM_{2.5}$ burden in Eastern China and 7–23% in Southern China during the three time periods.

In Eastern China, local emissions account for 27–40% of $PM_{2.5}$ column burden, while ROW contributes 20–45%. Southern China and Central-West China have 13–18% and 25–31% of local source contributions, respectively, whereas 37–64% are due to emissions from outside China in these two regions. In Southwestern China, 15–18% of the $PM_{2.5}$ burden originates from local emissions and 7–24% is from RCN. ROW emissions play important roles in affecting $PM_{2.5}$ burden over this region, with relative contributions in a range of 59–78% during the three time periods, which is associated with the transboundary transport by southwesterly winds. $PM_{2.5}$ burden over the Northwestern China and Himalayas and Tibetan Plateau with relatively low local emissions are strongly influenced by nonlocal sources, where more than 70% of the $PM_{2.5}$ burden originates from emissions outside China.

5.2 Aerosol source attribution during polluted days

In spite of the large reductions in emissions, severe air pollution events still occurred in China during the COVID-19 lockdown. Source attribution of $PM_{2.5}$ during polluted days in China has policy implications for future air pollution control. In Beijing, capital of China over the North China Plain, a serious haze event happened from February 11 to 13, 2020 during the COVID-19 outbreak period according to observations released by CNEMC. CAM5-EAST reproduced the polluted day on February 11 over the North China Plain. In this study, the most polluted day is defined as the day with the highest daily $PM_{2.5}$ concentration in February 2020 for each receptor region in China. Figure 7 presents the composite differences in near-surface $PM_{2.5}$ concentrations and 850 hPa wind fields between the most polluted day and normal days (all days in February 2020) for each receptor region. The local and nonlocal source contributions to the $PM_{2.5}$ differences are summarized in Fig. 8.

Unexpectedly, near-surface $PM_{2.5}$ concentrations in the North China

Plain and Eastern China experienced remarkable increases during the same most polluted day of COVID-19 lockdown. The simulated $PM_{2.5}$ concentrations increased, with the largest increases of more than 20 μg m^{-3} in the North China Plain and Eastern China, 10 μg m^{-3} maximum increase in the Southwestern China and 5 μg m^{-3} in the Northeastern, Southern and Central-West China, during the most polluted days compared to the normal days.

The increase in near-surface $PM_{2.5}$ concentrations during the most polluted day over Northeastern China is largely influenced by the local emissions, which contribute to a regional averaged concentration increase of 1.1 μg m^{-3}. This is mainly due to the accumulation of local aerosols under the weakened prevailing northwesterly winds over this region.

When the $PM_{2.5}$ pollution occurred in the North China Plain on February 11, 2020, which was also reported as the polluted day in observations (Huang et al., 2020), the concentration of $PM_{2.5}$ was 16.1 μg m^{-3} higher than that in normal days. The contribution from local emissions accounts for 66% of the averaged increase, which was related to the stagnant air condition (i.e., weakened lower tropospheric winds) resulting from the anomalous mid-tropospheric high pressure located at the climatological location of the East Asia trough (Fig. S5). Sources from Eastern China also explain 4.3 μg m^{-3} (27%) of the total increase over the North China Plain.

During the most polluted day in Eastern China (the same day as the most polluted day in North China Plain), the concentration of $PM_{2.5}$ was 16 $\mu g\ m^{-3}$ higher than that in normal days, which is primarily contributed by the local emissions. While the contribution from the North China Plain decreased in the most polluted day, the anomalous southerly winds brought more aerosols from Southern China and ROW into Eastern China, contributing to 4% and 10% aerosol increase, respectively.

Owing to the enhanced northerly winds, emissions from the North China Plain and Eastern China contribute 33% and 39% of the increase, respectively, in $PM_{2.5}$ concentration over Southern China. The most polluted day in Central-West China is mostly caused by local emissions (65% of the total increase).

When Southwestern China was under the polluted condition, $PM_{2.5}$ concentration increased by 2.1 $\mu g\ m^{-3}$. Emissions from ROW, especially those from South and Southeast Asia, are of great significance to the increase of $PM_{2.5}$ concentrations due to the enhanced southwesterly winds over this region. The relative contribution from ROW emissions is more than 50% over Southwestern China during the most polluted day. It highlights that the important role of transboundary transport needs to be considered when controlling local emissions to improve air quality in the near future.

6. Conclusions and discussions

The COVID-19 pandemic disrupted human activities and lead to abrupt reductions in anthropogenic emissions. This study first investigated the source contributions to $PM_{2.5}$ over various regions covering the whole China during the COVID-19 pandemic. We pay attention not only to local emissions, but also to the impacts from regional and foreign transport of aerosols. An explicit aerosol source tagging is implemented in the Community Atmosphere Model version 5 (CAM5-EAST) to examine the aerosol transport pathways and source attribution of $PM_{2.5}$ in China during the first few weeks of the COVID-19 outbreak (Week 1: January 30–February 5, Week 2: February 6–February 12 and Week 3: February 13–February 19). The contributions of emissions to $PM_{2.5}$ originating from eight source regions in the mainland of China, including Northeastern China, North China Plain, Eastern China, Southern China, Central-West China, Southwestern China, Northwestern China and Himalayas and Tibetan Plateau, and sources outside China (ROW) to near-surface concentrations, column burdens, transport pathways of $PM_{2.5}$, and haze formation in different receptor regions in China are quantified in this study.

Aerosols emitted from the North China Plain, where the air quality is often poor, can be transported through Eastern China and reach Southwestern China during the three time periods. Similarly, aerosols from Eastern China move straight to Southern China and Southwestern China during Week 1 and Week 2, and a significant portion can also enter the North China Plain during Week 2 and Week 3.

Across the southern boundary of the mainland of China, high concentrations of $PM_{2.5}$ from South and Southeast Asia are lifted into the free atmosphere and then transported to Southern and Southwestern China. While $PM_{2.5}$ from the North China Plain and Eastern China can also be brought out of China via westerly winds, mostly below 700 hPa.

$PM_{2.5}$ in China is affected not only by local emissions but also by long-range transport of pollutants from distant source regions. Over the North China Plain, 40–66% of the $PM_{2.5}$ burden is attributed to local emissions during the COVID-19 outbreak. They also impact $PM_{2.5}$ in neighboring regions, accounting for 14–33% of the $PM_{2.5}$ burden in Eastern China and 7–23% in Southern China during the three time periods. Northeastern China has 36%-43% of local source contributions to its $PM_{2.5}$ column burden, while 39%-54% is contributed by emissions from ROW during the three time periods. In Eastern China, local emissions explain 27–40% of $PM_{2.5}$ burden, while ROW contributes 20–45%. In Southwestern China, 59–78% of the $PM_{2.5}$ burden is contributed by emissions from ROW. Over the Northwestern China and Himalayas and Tibetan Plateau, ROW emissions have a great contribution of more than 70% to the $PM_{2.5}$ column burden.

In this study, the most polluted day is defined as the day with the highest daily $PM_{2.5}$ concentration in February 2020 for each receptor region in China. The transport from outside of China only has a great impact on some specific regions in China. In Southwestern China, the relative contribution from ROW emissions, especially those from South and Southeast Asia, to the increment of $PM_{2.5}$ concentration during the most polluted days compared with normal days is more than 50%. It is consistent with the previous studies that emissions from South and Southeast Asia have an important impact on air quality in southwest China (Yang et al., 2017a; Zhu et al., 2016, 2017). For other receptor regions in China (Northeastern China, North China Plain, Eastern China, Southern China and Central-West China), $PM_{2.5}$ concentrations are largely contributed by local emissions during the most polluted days compared with normal days. In the future with emissions reductions for better air quality in China, decreasing air pollution should consider aerosols from both Chinese local emissions and pollutant transport from outside of China.

Despite the large reductions in emissions, near-surface $PM_{2.5}$ concentrations in the North China Plain and Eastern China increased a lot during the most polluted days of COVID-19 lockdown (with the highest daily $PM_{2.5}$ concentration in February 2020), with the largest increases of more than 20 μg m^{-3}. In addition to local emissions, regional transport of pollutants is also an important factor that causes haze events in China. The increases in $PM_{2.5}$ concentrations during the most polluted days over the

North China Plain and Eastern China are largely influenced by the stagnant air condition resulting from the anomalous high pressure system and weakening of winds, which lead to a reduced ventilation and aerosol accumulation in the North China Plain, together with an increase in aerosol inflow from regional transport. During the most polluted day in Southwestern China, ROW contributes over 50% of the $PM_{2.5}$ concentration increase, with enhanced southwesterly winds that drive pollution transport from South and Southeast Asia. It indicates that regional transport and unfavorable meteorology need to be taken into consideration when controlling local emissions to improve air quality in the near future.

To highlight the roles of regional and foreign transport, the differences between Covid and Baseline simulations in relative contributions to $PM_{2.5}$ burden from local, region (RCN) and foreign (ROW) emissions are given in Figure S6. During the COVID-19 period, the local and RCN emission contributions to $PM_{2.5}$ were 1–4% lower than that in Base experiment over NCP and NEC. In Eastern China, the contribution from the local emissions decreased by 3–4% compared with Base experiment, while the contribution from ROW increased by more than 5%. In Southern China, 50–70% of the $PM_{2.5}$ burden is contributed by emissions from ROW in Base experiment. During the COVID-19 period with low emission levels, the contribution from ROW to $PM_{2.5}$ burden in Southern China had an increase of more than 5%. It indicates that the important role of transboundary transport needs to be considered when controlling local emissions to improve air quality in the near future.

Many studies have examined the importance of meteorology on regional air quality during the COVID-19 lockdown period and emphasized that, when meteorology is unfavorable, abrupt emissions reductions cannot avoid severe air pollutions (Le et al. 2020; Sulaymon et al. 2021; Shen et al. 2021). Through model simulations, Le et al. (2020) found that abnormally high humidity promotes the heterogeneous chemistry of aerosols, which have contributed to the increase of $PM_{2.5}$ by 12% in northern China during the city lockdown period. Sulaymon et al. (2021) found that significant increase in $PM_{2.5}$ concentrations caused by unfavorable meteorological conditions in Beijing-Tianjin-Hebei region during the lockdown period based on Community Multiscale Air Quality (CMAQ) model simulations. By analyzing the observational data and model simulations, Shen et al. (2021) reported that 50% of the pollution episodes during the COVID-19 lockdown in Hubei of China were due to the stagnant meteorological conditions. Huang et al. (2020) found that the stagnant air conditions and enhanced atmospheric oxidizing capacity caused a severe haze event during the same time period. In line with previous studies, we also revealed the stagnant air condition under the anomalous high pressure system in the most polluted day over the North China Plain. In addition to the meteorological conditions, the effect of foreign transport was also raised in this study causing aerosol pollution in southwestern China during COVID-19 outbreak.

There are a few uncertainties in this study. The CAM5 model has low biases in reproducing the near-surface $PM_{2.5}$ concentrations in China, compared to observations, in part due to the incapability of simulating some aerosol components of $PM_{2.5}$ (e.g., ammonium and nitrate), excessive aerosol wet removal during the long-range transport (Wang et al., 2013), and uncertainties in observations. In majority of the climate models, the simulation of nitrate and ammonium aerosols are not included in the aerosol schemes, partly due to the complexity of calculation efficiency. For example, in many of the CMIP6 models, only two of them provide nitrate and ammonium mass mixing ratios. Many previous studies have evaluated the global climate models performance in reproducing aerosol concentrations (e.g., Fan et al., 2018; Shindell et al., 2013; Yang et al., 2017a,b). In general, the models can well simulate aerosols in North America and Europe but significantly underestimates aerosols in East Asia by about −36 to −58 % compared with observations. It can lead to an underestimation of aerosols contributed by Chinese local emissions in magnitudes, but might not change the main conclusions of this study. Uncertainties in the estimate of emission reductions in different source regions during the COVID-19 pandemic can also introduce uncertainties to our results. During the COVID-19 lockdown, greenhouse gas emissions also decreased (Le Quéré et al., 2020), but the effect of greenhouse gas reduction on meteorology that potentially influence aerosol distributions was not taken into consideration. Nevertheless, this study is the first attempt to provide source apportionment of aerosols covering the whole China during the COVID-19 outbreak, which is beneficial to the investigation of policy implications for future air pollution control.

Data availability.

The CAM5 model is available at http://www.cesm.ucar.edu/models/cesm1.2/ (last access: 3 August 2021). CAM5-EAST model code and results can be made available upon request. The surface $PM_{2.5}$ observations are from the China National Environmental Monitoring Center (CNEMC, http://www.cnemc.cn, last access: 3 August 2021)

Competing interests.

The authors declare that they have no conflict of interest.

Author contribution.

YY and LR designed the research; YY performed the model simulations; LR analyzed the data. All authors discussed the results and wrote the paper.

Acknowledgments.

This study was supported by the National Key Research and Development Program of China (grant 2020YFA0607803 and 2019YFA0606800) and the National Natural Science Foundation of China (grant 41975159). HW acknowledges the support by the U.S. Department of Energy (DOE), Office of Science, Office of Biological and Environmental Research (BER). The Pacific Northwest National Laboratory (PNNL) is operated for DOE by the Battelle Memorial Institute under contract DE-AC05-76RLO1830.

Reference

Anderson, T.L., Charlson, R.J., Schwartz, S.E., Knutti, R., Boucher, O., Rodhe, H., Heintzenberg, J.: Climate forcing by aerosol–a hazy picture, Science, 300, 1103-1104, https://doi.org/10.1126/science.1084777, 2003.

Bao, R., Zhang, A.: Does lockdown reduce air pollution? Evidence from 44 cities in northern China, Sci. Total Environ., 731, 139052, https://doi.org/10.1016/j.scitotenv.2020.139052, 2020.

Chai, F., Gao, J., Chen, Z., Wang, S., Zhang, Y., Zhang, J., Zhang, H., Yun, Y., Ren, C.: Spatial and temporal variation of particulate matter and gaseous pollutants in 26 cities in China, J. Environ. Sci., 26, 75–82, https://doi.org/10.1016/S1001-0742(13)60383-6, 2014.

China State Council: Action Plan on Prevention and Control of Air Pollution, China State Council, Beijing, China, http://www.gov.cn/zwgk/2013-09/12/content_2486773.htm (last access: 27 September 2020), 2013.

Dong, E., Du, H., Gardner, L.: An interactive web-based dashboard to track COVID-19 in real time, Lancet Infect. Dis., 20, 533–534, https://doi.org/10.1016/S1473-3099(20)30120-1, 2020.

Fan, H., Zhao, C., Yang, Y.: A comprehensive analysis of the spatio-temporal variation of urban air pollution in China during 2014–2018, Atmos. Environ., 220, 117066, https://doi.org/10.1016/j.atmosenv.2019.117066, 2020.

Fan, T., Liu, X., Ma, P.-L., Zhang, Q., Li, Z., Jiang, Y., Zhang, F., Zhao, C., Yang, X., Wu, F., and Wang, Y.: Emission or atmospheric processes? An attempt to attribute the source of large bias of aerosols in eastern China simulated by global climate models, Atmos. Chem. Phys., 18, 1395–1417, https://doi.org/10.5194/acp-18-1395-2018, 2018.

Gelaro, R., McCarty, W., Suárez, M. J., Todling, R., Molod, A., Takacs, L., Randles, C. A., Darmenov, A., Bosilovich, M. G., Reichle, R., Wargan, K., Coy, L., Cullather, R., Draper, C., Akella, S., Buchard, V., Conaty, A., da Silva, A. M., Gu, W., Kim, G., Koster, R., Lucchesi, R., Merkova, D., Nielsen, J. E., Partyka, G., Pawson, S., Putman, W., Rienecker, M., Schubert, S. D., Sienkiewicz, M., Zhao, B.: The Modern-Era Retrospective Analysis for Research and Applications, Version 2 (MERRA-2), J. Climate, 30, 5419–5454, https://doi.org/10.1175/JCLI-D-16-0758.1, 2017.

Hadley, O. L., Ramanathan, V., Carmichael, G. R., Tang, Y., Corrigan, C. E., Roberts, G. C., Mauger, G. S.: Trans-Pacific transport of black carbon and fine aerosol ($D < 2.5\mu m$) into North America, J. Geophys. Res., 112, D05309, https://doi.org/10.1029/2006JD007632, 2007.

Heft-Neal, S., Burney, J., Bendavid, E., Burke, M.: Robust relationship between air quality and infant mortality in Africa, Nature, 559, 254. https://doi.org/10.1038/s41586-018-0263-3, 2018.

Hurrell, J. W., Holland, M. M., Gent, P. R., Ghan, S., Kay, J. E., Kushner, P. J., Lamarque, J. F., Large, W. G., Lawrence, D., Lind- say, K., Lipscomb, W. H., Long, M. C., Mahowald, N., Marsh, D. R., Neale, R. B., Rasch, P., Vavrus, S., Vertenstein, M., Bader, D., Collins, W. D., Hack, J. J., Kiehl, J., Marshall, S.: The Community Earth System Model A Framework for Collaborative Research, Bull. Am. Meteorol. Soc., 94, 1339–1360, https://doi.org/10.1175/BAMS-D-12-00121.1, 2013.

Huang, X., Ding, A., Gao, J., Zheng, B., Zhou, D., Qi, X., Tang, R., Ren, C., Nie, W., Chi, X., Wang, J., Xu, Z., Chen, L., Li, Y., Che, F., Pang, N., Wang, H., Tong, D., Qin, W., Cheng, W., Liu, W., Fu, Q., Chai, F., Davis, S. J., Zhang, Q., He, K.: Enhanced secondary pollution offset reduction of primary emissions during COVID-19 lockdown in China, Natl. Sci. Rev., nwaa137, https://doi.org/10.1093/nsr/nwaa137, 2020.

Kong, L., Feng, M., Liu, Y., Zhang, Y., Zhang, C., Li, C., Qu, Y., An, J., Liu, X., Tan, Q., Cheng, N., Deng, Y., Zhai, R., Wang, Z.: Elucidating the pollution characteristics of nitrate, sulfate and ammonium in PM2.5 in Chengdu, southwest China, based on 3-year measurements, Atmos. Chem. Phys., 20, 11181–11199, https://doi.org/10.5194/acp-20-11181-2020, 2020.

Le, T., Wang, Y., Liu, L., Yang, J., Yung, Y. L., Li, G., Seinfeld, J. H.: Unexpected air pollution with marked emission reductions during the COVID-19 outbreak in China, Science, 369, 702–706, https://doi.org/10.1126/science.abb7431, 2020.

Le Quéré, C., Jackson, R. B., Jones, M. W., Smith, A. J. P., Abernethy, S., Andrew, R. M., De-Gol, A. J., Willis, D. R., Shan, Y. L., Canadell, J. G., Friedlingstein, P., Felix Creutzig, F., Peters, G.,P.: Temporary reduction in daily global CO2 emissions during the COVID-19 forced confinement, Nat. Clim. Chang., 10, 647–653, https://doi.org/10.1038/s41558-020-0797-x, 2020.

Lelieveld, J., Klingmüller, K., Pozzer, A., Burnett, R. T., Haines, A., Ramanathan,V.: Effects of fossil fuel and total anthropogenic emission removal on public health and climate. P. Natl. Acad. Sci., 116, 7192–7197, https://doi.org/10.1073/pnas.1819989116, 2019.

Liao, H., Chang, W., Yang, Y.: Climatic effects of air pollutants over China: A review, Adv. Atmos. Sci., 32, 115–139, https://doi.org/10.1007/s00376-014-0013-x, 2015.

Li, L., Li, Q., Huang, L., Wang, Q., Zhu, A., Xu, J., Liu, Z., Li, H., Shi, L., Li, R., Azari, M., Wang, Y., Zhang, X., Liu, Z., Zhu, Y., Zhang, K., Xue, S., Ooi, M., C., G., Zhang, D., Chan, A.: Air quality changes during the COVID-19 lockdown over the Yangtze River Delta Region: An insight into the impact of human activity pattern changes on air pollution variation. Sci. Total Environ., 732, 139282. https://doi.org/10.1016/j.scitotenv.2020.139282, 2020.

Liu, X., Easter, R. C., Ghan, S. J., Zaveri, R., Rasch, P., Shi, X., Lamarque, J., F., Gettelman, A., Morrison, H., Vitt, F., Conley, A., Park, S., Neale, R., Hannay, C., Ekman, A. M. L., Hess, P., Mahowald, N., Collins, W., Iacono, M. J., Bretherton, C. S., Flanner, M. G., Mitchell, D.: Toward a minimal representation of aerosols in climate models: description and evaluation in the Community Atmosphere Model CAM5, Geosci. Model Dev., 5, 709–739. https://doi.org/10.5194/gmd-5-709-2012, 2012.

Liu, Y., Hong, Y., Fan, Q., Wang, X., Chan, P., Chen, X., Lai, A., Wang, M., Chen, X.: Source-receptor relationships for $PM_{2.5}$ during typical pollution episodes in the Pearl River Delta city cluster, China, Sci. Total Environ., 596, 194-206, https://doi.org/10.1016/j.scitotenv.2017.03.255, 2017.

Lund, M. T., Myhre, G., and Samset, B. H.: Anthropogenic aerosol forcing under the Shared Socioeconomic Pathways, Atmos. Chem. Phys., 19, 13827–13839, https://doi.org/10.5194/acp-19-13827-2019, 2019.

Lyakaremye, V., Zeng, G., Siebert, A., Yang, X.: Contribution of external forcings to the observed trend in surface temperature over Africa during 1901–2014 and its future projection from CMIP6 simulations, Atmos. Res., 254, 105512, https://doi.org/10.1016/j.atmosres.2021.105512, 2021.

Ramanathan, V. C. P. J., Crutzen, P. J., Kiehl, J. T., Rosenfeld, D.: Aerosols, climate, and the hydrological cycle, science, 294, 2119-2124, https://doi.org/10.1126/science.1064034, 2001.

Ren, L., Yang, Y., Wang, H., Zhang, R., Wang, P., Liao, H.: Source attribution of Arctic aerosols and associated Arctic warming trend during 1980–2018, Atmos. Chem. Phys., 20, 9067-9085, https://doi.org/10.5194/acp-2020-3,2020.

Sharma, S., Zhang, M., Anshika, Gao, J., Kota, S. H.: Effect of restricted emissions during covid-19 on air quality in india, Sci. Total Environ., 728, 138878, https://doi.org/10.1016/j.scitotenv.2020.138878, 2020.

Shen, L., Zhao, T., Wang, H., Liu, J., Bai, Y., Kong, S., Zheng, H., Zhu, Y., Shu, Z.: Importance of meteorology in air pollution events during the city lockdown for COVID-19 in Hubei Province, Central China, Sci. Total Environ., 754, 142227, https://doi.org/10.1016/j.scitotenv.2020.142227, 2021.

Shindell, D. T., Lamarque, J.-F., Schulz, M., Flanner, M., Jiao, C., Chin, M., Young, P. J., Lee, Y. H., Rotstayn, L., Mahowald, N., Milly, G., Faluvegi, G., Balkanski, Y., Collins, W. J., Conley, A. J., Dalsoren, S., Easter, R., Ghan, S., Horowitz, L., Liu, X., Myhre, G., Nagashima, T., Naik, V., Rumbold, S. T., Skeie, R., Sudo, K., Szopa, S., Takemura, T., Voulgarakis, A., Yoon, J.-H., and Lo, F.: Radiative forcing in the ACCMIP historical and future climate simulations, Atmos. Chem. Phys., 13, 2939–2974, https://doi.org/10.5194/acp-13-2939-2013, 2013.

Smith, C. J., Kramer, R. J., Myhre, G., Alterskjær, K., Collins, W., Sima, A., Boucher, O., Dufresne, J.-L., Nabat, P., Michou, M., Yukimoto, S., Cole, J., Paynter, D., Shiogama, H., O'Connor, F.

M., Robertson, E., Wiltshire, A., Andrews, T., Hannay, C., Miller, R., Nazarenko, L., Kirkevåg, A., Olivié, D., Fiedler, S., Lewinschal, A., Mackallah, C., Dix, M., Pincus, R., Forster, P. M.: Effective radiative forcing and adjustments in CMIP6 models, Atmos. Chem. Phys.,20, 9591–9618, https://doi.org/10.5194/acp-20-9591-2020, 2020.

Sulaymon, I. D., Zhang, Y., Hopke, P. K., Hu, J., Zhang, Y., Li, L., Mei, X., Gong, K., Shi, Z., Zhao, B., Zhao, F.: Persistent high PM2.5 pollution driven by unfavorable meteorological conditions during the COVID-19 lockdown period in the Beijing-Tianjin-Hebei region, China, Environ. Res., 198, 111186, https://doi.org/10.1016/j.envres.2021.111186, 2021.

Tian, H., Liu, Y., Li, Y.,Wu, C., Chen, B., Kraemer, M.U.G., Li, B., Cai, J., Xu, B., Yang, Q.,Wang, B., Yang, P., Cui, Y., Song, Y., Zheng, P.,Wang, Q., Bjornstad, O.N., Yang, R., Grenfell, B.T., Pybus, O.G., Dye, C.: An investigation of transmission control measures during the first 50 days of the COVID-19 epidemic in China, Science, b6105 https://doi.org/10.1126/science.abb6105, 2020.

Vautard, R., Yiou, P., Oldenborgh, G.: Decline of fog, mist and haze in Europe over the past 30 years, Nat. Geosci., 2, 115–119, https://doi.org/10.1038/ngeo414, 2009.

Wang, H., Easter, R. C., Rasch, P. J., Wang, M., Liu, X., Ghan, S. J., Qian, Y., Yoon, J.-H., Ma, P.-L., Vinoj, V.: Sensitivity of remote aerosol distributions to representation of cloud–aerosol interactions in a global climate model, Geosci. Model Dev., 6, 765–782, https://doi.org/10.5194/gmd-6-765-2013, 2013.

Wang, H., Rasch, P. J., Easter, R. C., Singh, B., Zhang, R., Ma, P. L., Qian, Y., Ghan, S. J., Beagley, N.: Using an explicit emission tagging method in global modeling of source-receptor relationships for black carbon in the Arctic: Variations, sources, and transport pathways, J. Geophys. Res., 119, 12888–12909, https://doi.org/10.1002/2014JD022297, 2014.

Wang, H., Easter, R. C., Zhang, R., Ma, P., Singh, B., Zhang, K., Ganguly, D., Rasch, P. J., Burrows, S. M., Ghan, S. J., Lou, S., Qian, Y., Yang, Y., Feng, Y., Flanner, M., Leung, L. R., Liu, X., Shrivastava, M., Sun, J., Tang, Q., Xie, S., Yoon, J.: Aerosols in the E3SM Version 1: New Developments and Their Impacts on Radiative Forcing, J. Adv. Model. Earth Sy., 12, 293, https://doi.org/10.1029/2019MS001851, 2020.

Wang, P., Chen, K., Zhu, S., Wang, P., Zhang, H.: Severe air pollution events not avoided by reduced anthropogenic activities during COVID-19 outbreak, Resour. Conserv. Recycl., 158, 104814, https://doi.org/10.1016/j.resconrec.2020.104814, 2020.

Wang, Q., Huang, R. J., Cao, J., Tie, X., Shen, Z., Zhao, S., Han, Y., Li, G., Li, Z., Ni, H., Zhou, Y., Wang, M., Chen, Y., Zhou, Y.: Contribution of regional transport to the black carbon aerosol during winter haze period in Beijing, Atmos. Environ., 132,11-28, https://doi.org/10.1016/j.atmosenv.2016.02.031, 2016.

Watson, J. G.: Visibility: Science and regulation. J. Air Waste Manage. Assoc., 52, 628-713, https://doi.org/10.1080/10473289.2002.10470813, 2002.

Xu, Q., Wang, S., Jiang, J., Bhattarai, N., Li, X., Chang, X., Qiu, X., Zheng, M., Hua, Y., Hao, J.: Nitrate dominates the chemical composition of $PM_{2.5}$ during haze event in Beijing, China, Sci. Total Environ., 689, 1293–1303. https://doi.org/10.1016/j.scitotenv.2019.06.294, 2019.

Xue, W. B., Fu, F., Wang, J. N., Tang, G. Q., Lei, Y., Yang, J. T., Wang, Y. S.: Numerical study on the characteristics of regional transport of PM2.5 in China, J. Environ. Sci., 34, 1361–1368, 2014.

Yang, Y., Wang, H., Smith, S. J., Ma, P. L., Rasch, P. J.: Source attribution of black carbon and its direct radiative forcing in China, Atmos. Chem. Phys., 17, 4319–4336, https://doi.org/10.5194/acp-17-4319-2017, 2017a.

Yang, Y., Wang, H., Smith, S. J., Easter, R., Ma, P. L., Qian, Y., Yu, H., Li, C., Rasch, P. J.: Global source attribution of sulfate concentration and direct and indirect radiative forcing, Atmos. Chem. Phys., 17, 8903–8922, https://doi.org/10.5194/acp-17-8903-2017, 2017b.

Yang, Y., Wang, H., Smith, S. J., Zhang, R., Lou, S., Qian, Y., Ma, P.-L., Rasch, P. J.: Recent intensification of winter haze in China linked to foreign emissions and meteorology, Sci. Rep., 8, 2107, https://doi.org/10.1038/s41598-018-20437-7, 2018a.

Yang, Y., Wang, H., Smith, S. J., Easter, R. C., Rasch, P. J.: Sulfate aerosol in the Arctic: Source attribution and radiative forcing, J. Geophys. Res., 123, 1899–1918, https://doi.org/10.1002/2017JD027298, 2018b.

Yang, Y., Wang, H., Smith, S. J., Zhang, R., Lou, S., Yu, H., Li, C., Rasch, P. J.: Source apportionments of aerosols and their direct radiative forcing and long-term trends over continental United States, Earth's Future, 6, 793–808, https://doi.org/10.1029/2018EF000859, 2018c.

Yang, Y., Smith, S. J., Wang, H., Lou, S., Rasch, P. J.: Impact of anthropogenic emission injection height uncertainty on global sulfur dioxide and aerosol distribution, J. Geophys. Res., 124, 4812–4826, https://doi.org/10.1029/2018JD030001, 2019a.

Yang, Y., Smith, S. J., Wang, H., Mills, C. M., Rasch, P. J.: Variability, timescales, and nonlinearity in climate responses to black carbon emissions, Atmos. Chem. Phys., 19, 2405–2420, https://doi.org/10.5194/acp-19-2405-2019, 2019b.

Yang, Y., Lou, S., Wang, H., Wang, P., Liao, H.: Trends and source apportionment of aerosols in Europe during 1980–2018, Atmos. Chem. Phys., 20, 2579–2590, https://doi.org/10.5194/acp-20-2579-2020, 2020.

Yu, H. B., Remer, L. A., Chin, M., Bian, H. S., Tan, Q., Yuan, T. L., Zhang, Y.: Aerosols from overseas rival domestic emissions over North America, Science, 337, 566–569, https://doi.org/10.1126/science.1217576, 2012.

Yu, H., Remer, L. A., Chin, M., Bian, H., Kleidman, R. G., Diehl, T.: A satellite-based assessment of transpacific transport of pollution aerosol, J. Geophys. Res., 113, D14S12, https://doi.org/10.1029/2007JD009349, 2008.

Zhang, R., Wang, H., Hegg, D. A., Qian, Y., Doherty, S. J., Dang, C., Ma, P. L., Rasch, P. J., Fu, Q.: Quantifying sources of black carbon in western North America using observationally based analysis and an emission tagging technique in the Community Atmosphere Model, Atmos. Chem. Phys., 15, 12,805–12,822, https://doi.org/10.5194/acpd-15-12957-2015, 2015.

Zheng, B., Tong, D., Li, M., Liu, F., Hong, C., Geng, G., Li, H., Li, X., Peng, L., Qi, J., Yan, L., Zhang, Y., Zhao, H., Zheng, Y., He, K., Zhang, Q.: Trends in China's anthropogenic emissions since 2010 as the consequence of clean air actions, Atmos. Chem. Phys.s, 18, 14095–14111, https://doi.org/10.5194/acp-18-14095-2018, 2018.

Zhuang, B. L., Li, S., Wang, T. J., Liu, J., Chen, H. M., Chen, P. L., Li, M. M., Xie, M.: Interaction between the Black Carbon Aerosol Warming Effect and East Asian Monsoon Using RegCM4, J. Climate, 31, 9367-9388, https://doi.org/10.1175/JCLI-D-17-0767.1, 2018.

Zhu, J., Xia, X., Che, H., Wang, J., Zhang, J., Duan, Y.: Study of aerosol optical properties at Kunming in southwest China and longrange transport of biomass burning aerosols from North Burma, Atmos. Res., 169, 237–247, https://doi.org/10.1016/j.atmosres.2015.10.012, 2016.

Zhu, J., Xia, X., Wang, J., Zhang, J., Wiedinmyer, C., Fisher, J. A., Keller, C. A.: Impact of Southeast Asian smoke on aerosol properties in Southwest China: First comparison of model simulations with satellite and ground observations, J. Geophys. Res. Atmos., 122, 3904–3919, https://doi.org/10.1002/2016JD025793, 2017.

Table 1. Fractional contributions of emissions from nine tagged source regions (vertical axis) to mean $PM_{2.5}$ column burden in eight receptor regions (horizontal axis) during the three time periods ('Week 1': January 30–February 5, 'Week 2': February 6–February 12 and 'Week 3': February 13–February 19).

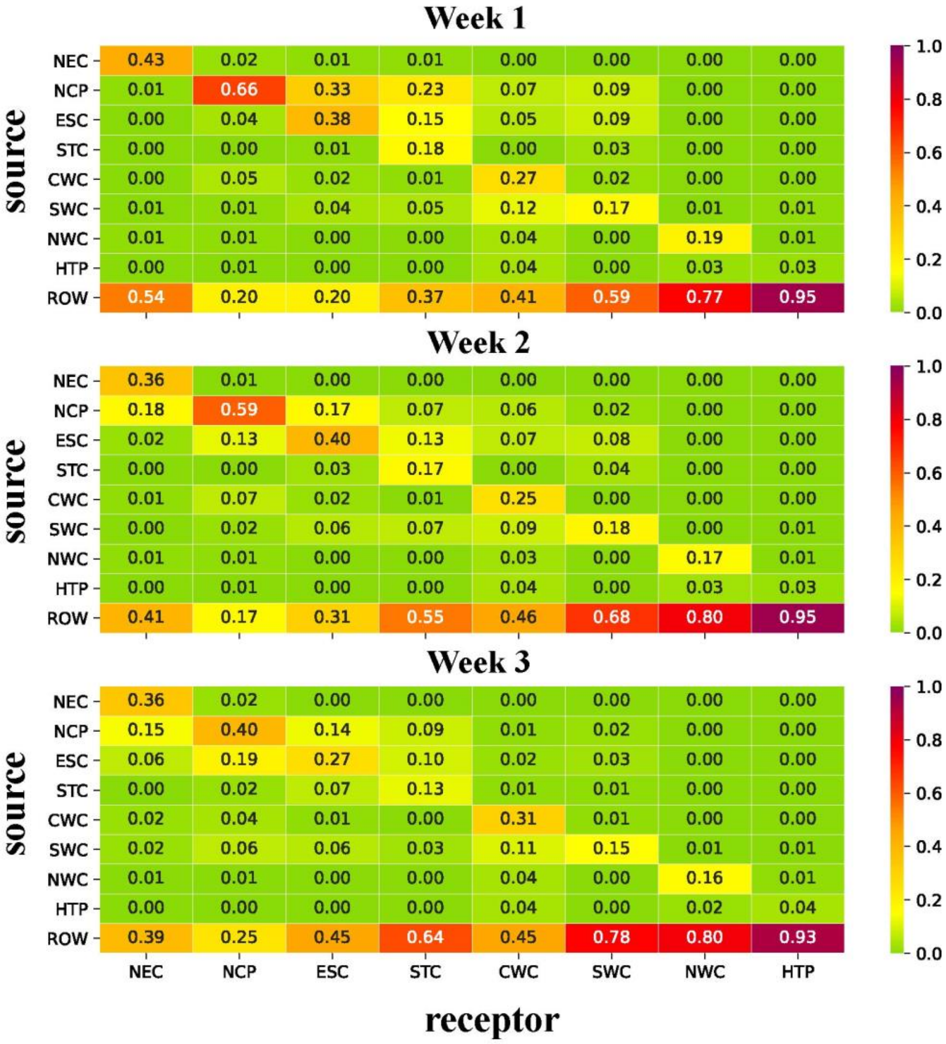

Week 1

source \ receptor	NEC	NCP	ESC	STC	CWC	SWC	NWC	HTP
NEC	0.43	0.02	0.01	0.01	0.00	0.00	0.00	0.00
NCP	0.01	0.66	0.33	0.23	0.07	0.09	0.00	0.00
ESC	0.00	0.04	0.38	0.15	0.05	0.09	0.00	0.00
STC	0.00	0.00	0.01	0.18	0.00	0.03	0.00	0.00
CWC	0.00	0.05	0.02	0.01	0.27	0.02	0.00	0.00
SWC	0.01	0.01	0.04	0.05	0.12	0.17	0.01	0.01
NWC	0.01	0.01	0.00	0.00	0.04	0.00	0.19	0.01
HTP	0.00	0.01	0.00	0.00	0.04	0.00	0.03	0.03
ROW	0.54	0.20	0.20	0.37	0.41	0.59	0.77	0.95

Week 2

source \ receptor	NEC	NCP	ESC	STC	CWC	SWC	NWC	HTP
NEC	0.36	0.01	0.00	0.00	0.00	0.00	0.00	0.00
NCP	0.18	0.59	0.17	0.07	0.06	0.02	0.00	0.00
ESC	0.02	0.13	0.40	0.13	0.07	0.08	0.00	0.00
STC	0.00	0.00	0.03	0.17	0.00	0.04	0.00	0.00
CWC	0.01	0.07	0.02	0.01	0.25	0.00	0.00	0.00
SWC	0.00	0.02	0.06	0.07	0.09	0.18	0.00	0.01
NWC	0.01	0.01	0.00	0.00	0.03	0.00	0.17	0.01
HTP	0.00	0.01	0.00	0.00	0.04	0.00	0.03	0.03
ROW	0.41	0.17	0.31	0.55	0.46	0.68	0.80	0.95

Week 3

source \ receptor	NEC	NCP	ESC	STC	CWC	SWC	NWC	HTP
NEC	0.36	0.02	0.00	0.00	0.00	0.00	0.00	0.00
NCP	0.15	0.40	0.14	0.09	0.01	0.02	0.00	0.00
ESC	0.06	0.19	0.27	0.10	0.02	0.03	0.00	0.00
STC	0.00	0.02	0.07	0.13	0.01	0.01	0.00	0.00
CWC	0.02	0.04	0.01	0.00	0.31	0.01	0.00	0.00
SWC	0.02	0.06	0.06	0.03	0.11	0.15	0.01	0.01
NWC	0.01	0.01	0.00	0.00	0.04	0.00	0.16	0.01
HTP	0.00	0.00	0.00	0.00	0.04	0.00	0.02	0.04
ROW	0.39	0.25	0.45	0.64	0.45	0.78	0.80	0.93

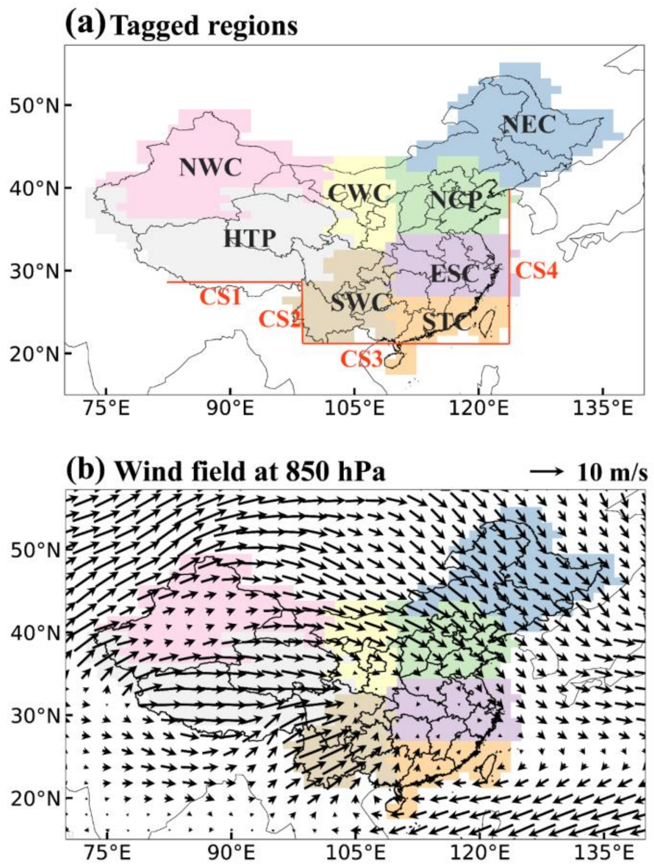

Figure 1. (a) Tagged source regions (NEC: Northeastern China, NCP: North China Plain, ESC: Eastern China, STC: Southern China, CWC: Central-West China, SWC: Southwestern China, NWC: Northwestern China, HTP: Himalayas and Tibetan Plateau, ROW: rest of the world) and (b) mean wind field (units: m s^{-1}, vectors) at 850 hPa during the three weeks of the study from January 30 to February 19, which had the largest number of newly-diagnosed COVID-19 cases. Lines in (a) mark the cross-sections (CS) defined to study the transport of aerosols to and from China.

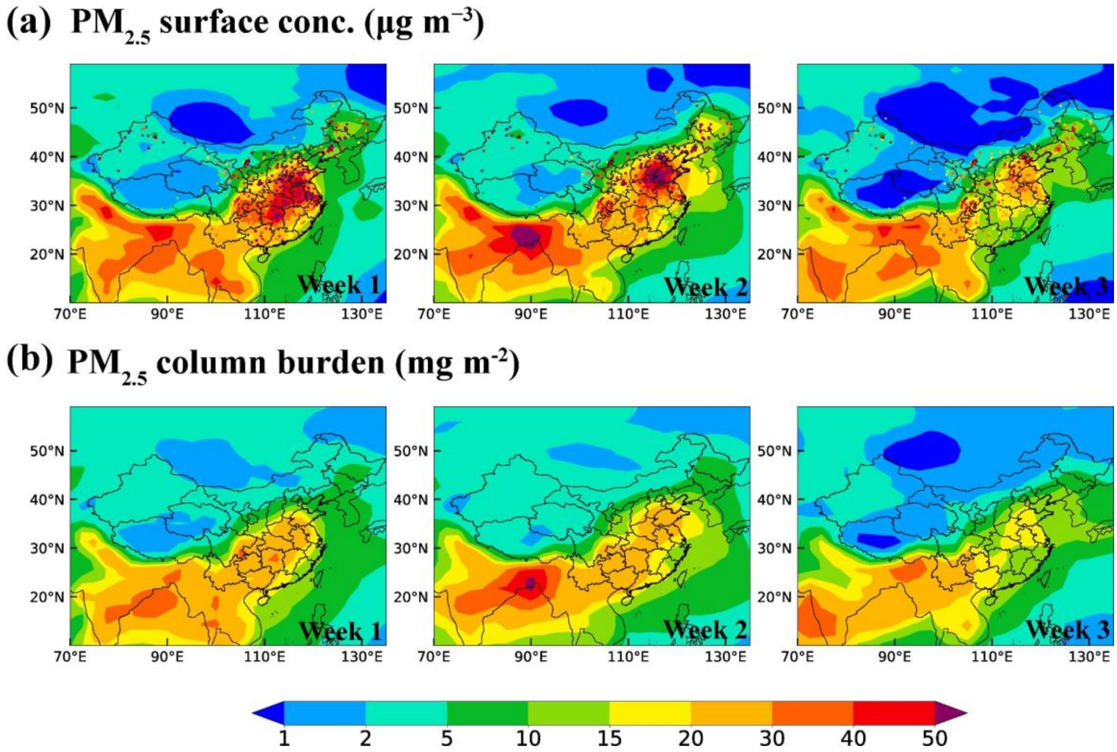

Figure 2. Spatial distribution of (a) the simulated and observed mean near-surface $PM_{2.5}$ concentrations (μg m^{-3}) and (b) $PM_{2.5}$ column burden (mg m^{-2}) during January 30–February 5 (Week 1), February 6–February 12 (Week 2) and February 13–February 19 (Week 3).

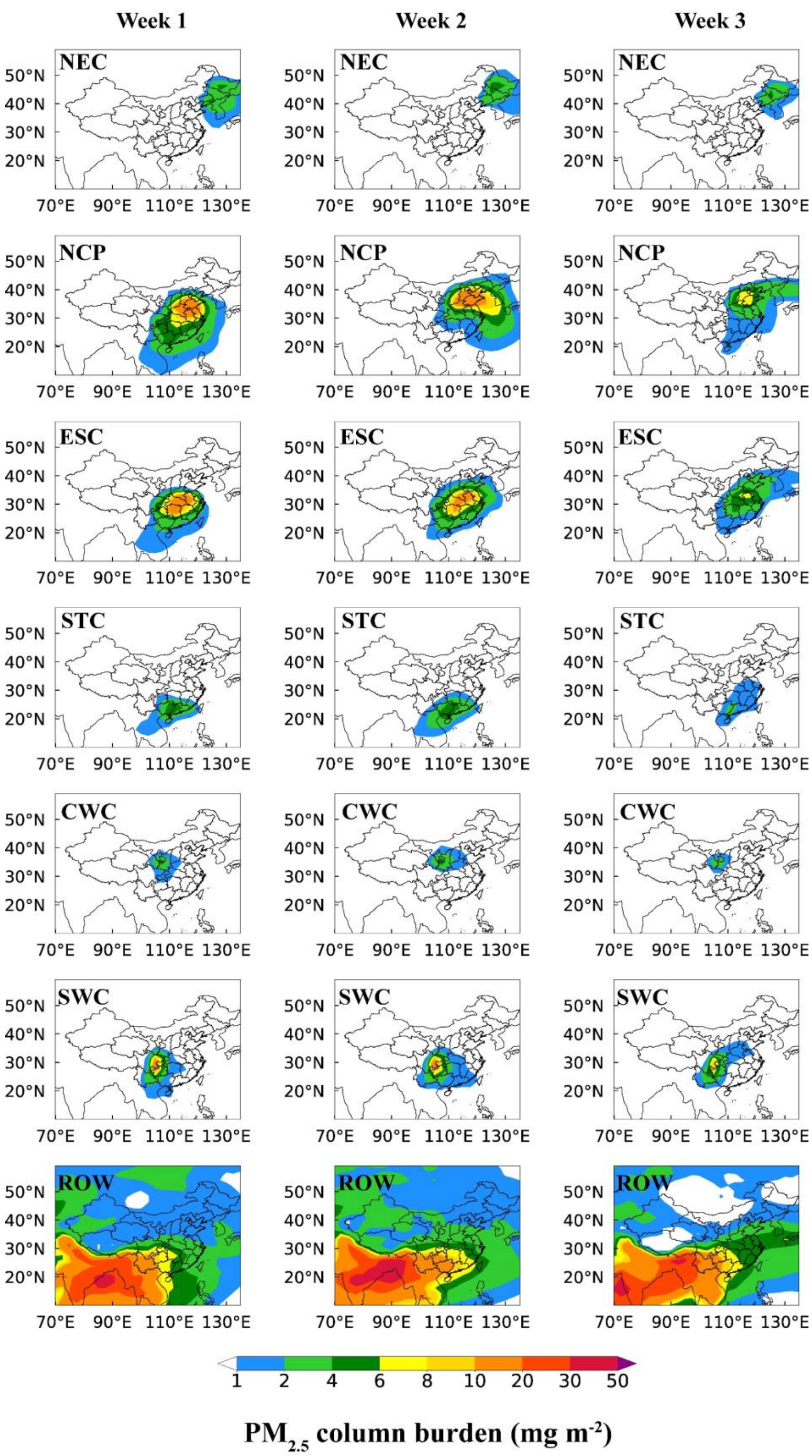

Figure 3. Spatial distribution of $PM_{2.5}$ column burden (mg m^{-2}) originating from the six major source regions in China (NEC, NCP, ESC, STC, CWC and SWC) and sources outside China (ROW) during the three time periods.

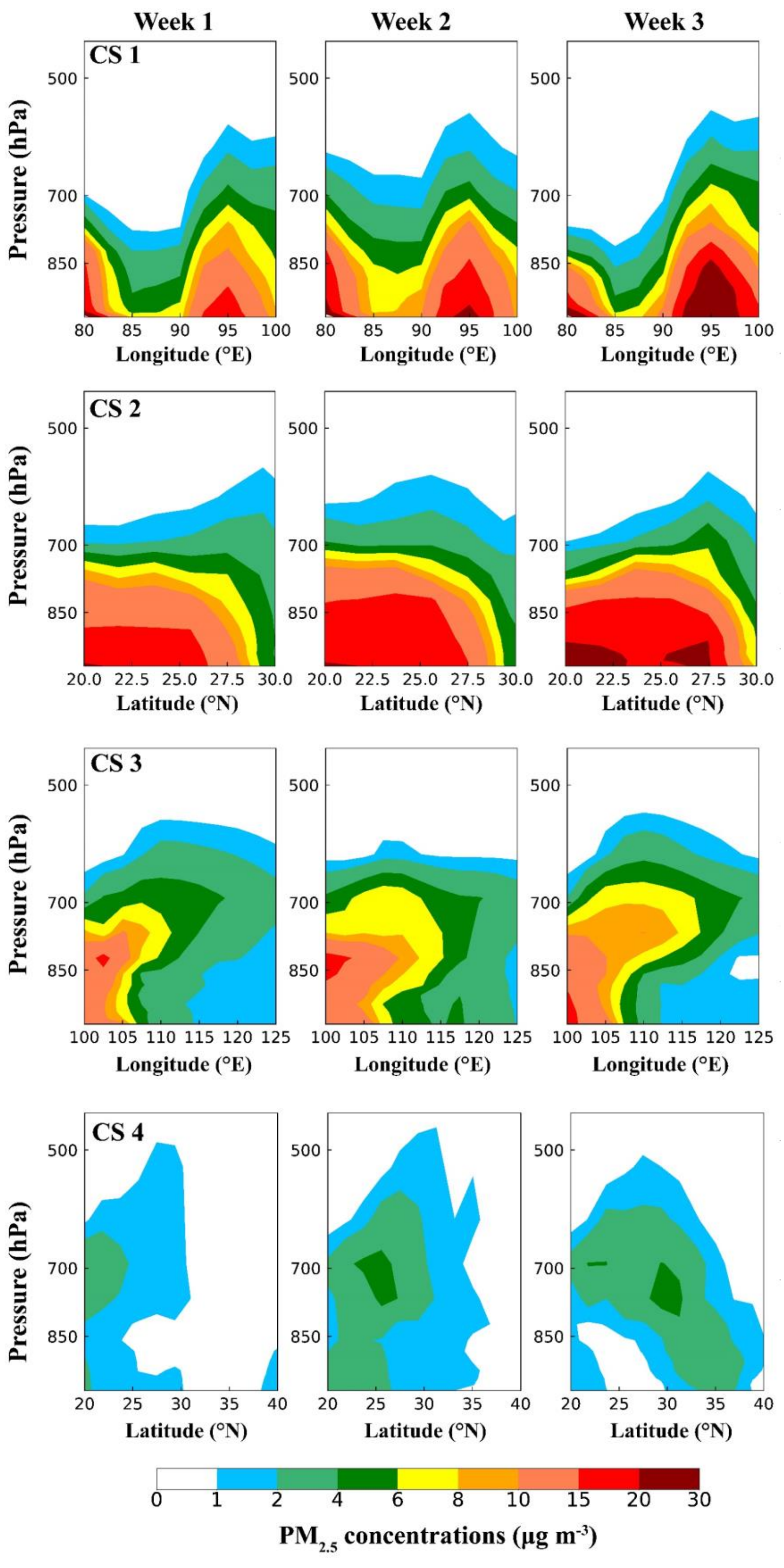

Figure 4. Vertical distributions of $PM_{2.5}$ concentrations (μg m^{-3}), originating from emissions outside China (i.e., ROW sources), across the latitudinal and/or longitudinal extents marked in Fig.1, respectively, during the three time periods.

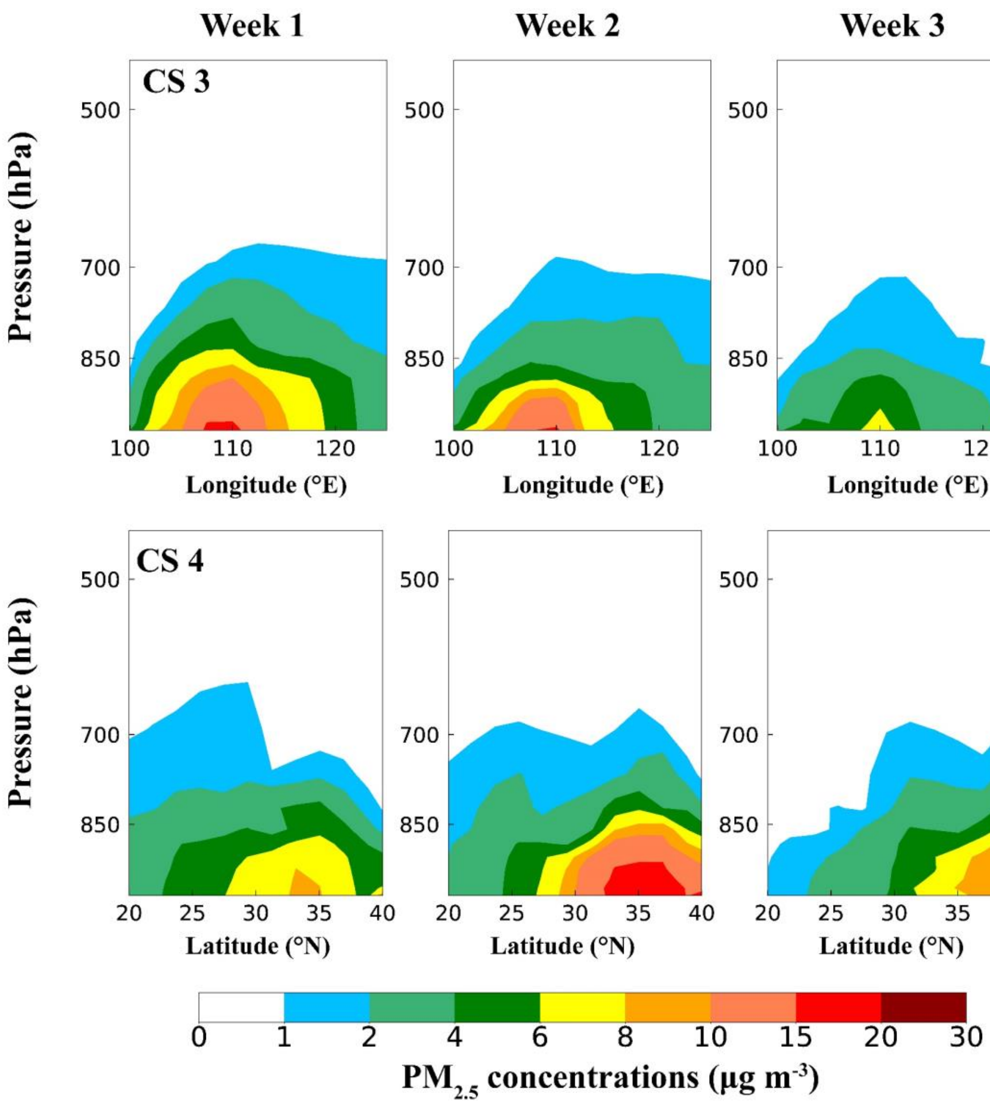

Figure 5. Vertical distributions of $PM_{2.5}$ concentrations (μg m^{-3}), originating from domestic emissions in China, across the latitudinal and/or longitudinal extents marked in Fig.1, respectively, during the three time periods. The values along CS 1 and CS 2 are negligibly small.

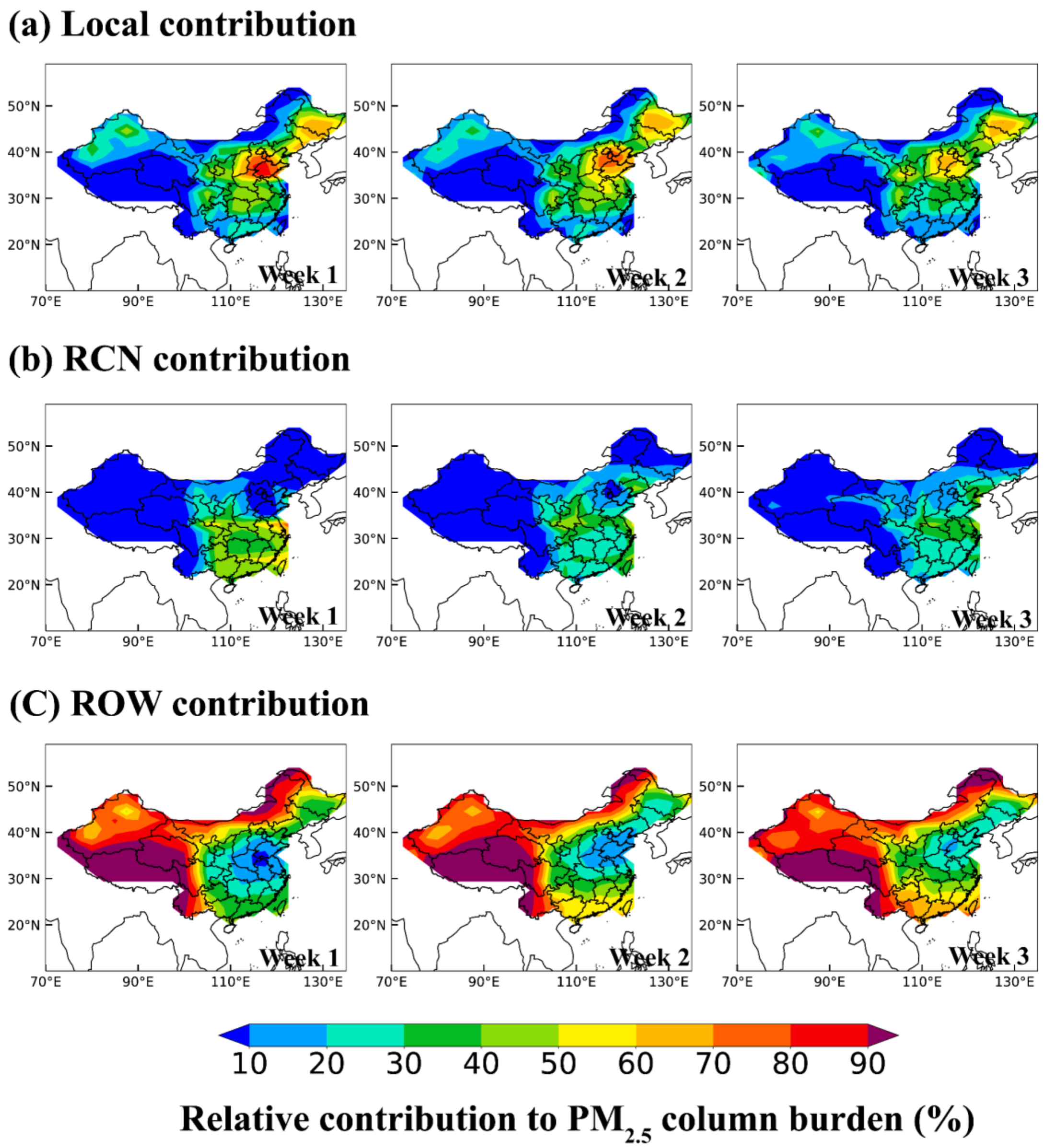

Figure 6. Relative contributions (%) of (a) local emissions, (b) the emissions from the rest of China (RCN) and (c) all sources outside China (rest of the world, ROW) to $PM_{2.5}$ column burden during the three time periods.

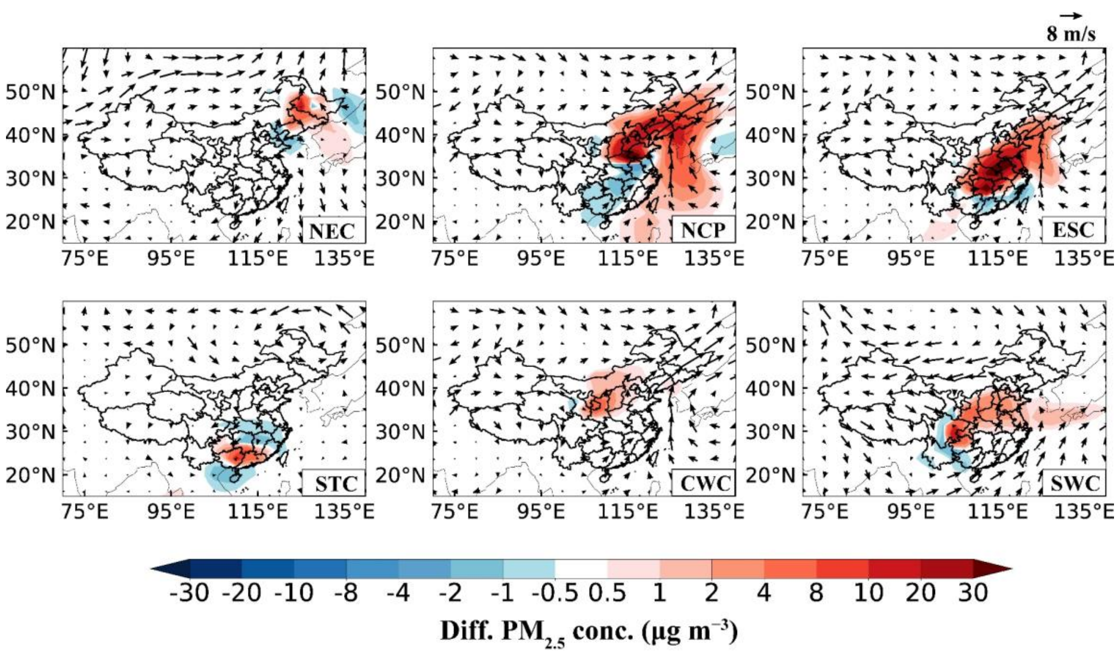

Figure 7. Composite differences in winds at 850 hPa (m s^{-1}) and near-surface $PM_{2.5}$ concentrations (μg m^{-3}) between the most polluted and normal days in February 2020. The most polluted day is defined as the day with the highest daily $PM_{2.5}$ concentration in February 2020 in each receptor region in China.

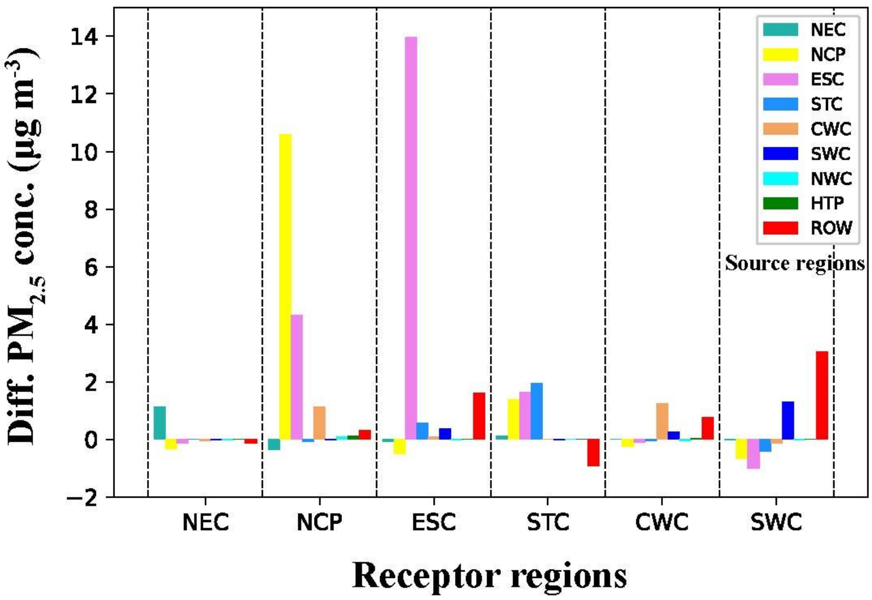

Figure 8. Composite differences in near-surface $PM_{2.5}$ concentrations (μg m^{-3}) averaged over receptor regions (marked on the horizontal axis) in China between the most polluted and normal days in February 2020 originating from individual source regions (corresponding color bars in each column).